RSC Advances

PAPER

View Article Online
View Journal | View Issue

Cite this: *RSC Adv.*, 2019, **9**, 17812

PdAu alloy nanoparticles supported on nitrogen-doped carbon black as highly active catalysts for Ullmann coupling and nitrophenol hydrogenation reactions†

Fengyan Han, ‡*[ab] Jiawei Xia,‡[a] Xinglong Zhang[b] and Yongsheng Fu[a]

Noble metal-based catalysts have been proven to be active for catalytic organic reactions. The selectivity and conversion can be improved by integration with proper carrier materials, and further modulated by tuning the composition as well as the electronic structure of the active noble metals. Compared with unsupported monometallic catalysts, the synergistic interactions between neighboring metals and the combined effects between the carrier materials and the active components often give rise to positive influences on the enhancement of the catalytic efficiency and selectivity. In this work, we report a facile process for the fabrication of nitrogen-doped carbon black (NCB) supported PdAu bimetallic nanoparticles (NPs) with a uniform dispersion and narrow size distribution. The PdAu/NCB catalyst with a Pd/Au mole ratio of 1/1 shows the highest activity towards both Ullmann coupling reactions of aryl halides and the hydrogenation reaction of nitrophenols. Moreover, this bimetallic catalyst also exhibits a superior recycling durability to that of monometallic Pd/NCB and Au/NCB catalysts. The enhanced catalytic performance of the bimetallic catalyst is mainly due to the large BET specific surface area (125.45 m^2 g^{-1}) and the synergy between the individual components of the catalyst.

Received 6th March 2019
Accepted 16th May 2019

DOI: 10.1039/c9ra01685f

rsc.li/rsc-advances

Introduction

The synthesis of symmetrical di- or poly-aromatic compounds is one of the important processes in industry, and shows a wide application in the production of pharmaceuticals, natural products and organic conductors.[1–3] The Pd-catalyzed Suzuki, Stille, Negishi and Ullmann coupling reactions are commonly used for the fabrication of carbon–carbon bonds to generate biaromatic compounds.[4–7] Among the reactions above, the homogeneous Ullmann coupling of aryl halides is one of the most versatile strategies for the synthesis of symmetrical biaromatic compounds. However, the traditional homogeneous Ullmann coupling reaction is always carried out at a relatively high temperature in an organic medium with a high boiling point, leading to extensive energy-consumption and complicated post-processing. Hence, the development of highly efficient catalysts and the exploration of mild reaction conditions are in great demand. Even though a variety of homogeneous catalysts have been explored recently for homogeneous Ullmann coupling reactions,[8–11] the exorbitant price of the complex catalysts, non-recyclable property and complicated post-processing are still the main blocks for such a homogeneous catalysis.

To date, with the rapid development of nanotechnology, more and more attention has been paid to the design and synthesis of nanomaterials with unique structures as catalysts for organic reactions. Metallic NPs were widely studied in the areas of the hydrogenation reaction, coupling reaction, *etc.*[12,13] Compared with monometallic NPs, multimetallic NPs often reveal enhanced optical, electronic and catalytic activity on account of the synergistic effect between different metal atoms.[14–18] As a result, remarkable progress was achieved in the controllable synthesis and potential applications of bimetallic catalysts on the basis of a well-understood design strategy. The most studied bimetallic catalysts, such as Pd-based bimetallic catalysts, including Pd–Au,[19,20] Pd–Ni,[21] Pd–Ag[22] and Pd–Cu,[23] have been widely investigated for varied catalytic applications in oxidation, reduction and coupling reactions. Among these bimetallic catalysts, bimetallic PdAu materials have attracted extensive attention in the field of heterogeneous Ullmann coupling reactions due to their excellent catalytic activity and durability. For example, Sakurai *et al.* synthesized bimetallic Au/Pd nanoclusters for the Ullmann coupling of chloroarenes under an argon atmosphere at a low temperature with a high yield.[24] Wang and co-workers prepared Au–Pd alloyed

[a]*Key Laboratory for Soft Chemistry and Functional Materials of Ministry Education, Nanjing University of Science and Technology, Nanjing 210094, China*

[b]*College of Science, Institute of Materials Physics and Chemistry, Nanjing Forestry University, Nanjing 210037, China. E-mail: fengyanhan@njfu.edu.cn*

† Electronic supplementary information (ESI) available. See DOI: 10.1039/c9ra01685f

‡ These authors contributed equally to this work.

nanochain networks by using 4-aminopyridine as the structure-directing agent for the Ullmann intermolecular and intramolecular homocoupling and the catalyst exhibited a high activity and good stability.[25]

It is reported that the combination of active components with some certain carrier materials can largely improve the activity and stability of the catalysts. The carrier materials can help disperse the active components and prevent their aggregation, and meanwhile reduce the dosage of active components, especially for the precious metals, which is in favor of a controlled catalysis cost. Among various carrier materials, such as hydrotalcite,[26] graphitic carbon nitride,[27] metal–organic frameworks,[28] graphene[29,30] and carbon materials,[31] XC-72 carbon black is one of the most promising in the near future because of many admirable properties, such as permeable pores, large surface area, excellent conductivity, good stability and chemical inertness.[32–34] As reported, nitrogen doping is considered one of the most effective ways to further modify the properties of carbon materials, where the more negatively-charged nitrogen atoms can help to gain interactions between the active components and the substrates.[35–39] The lone pair electrons in the nitrogen atoms can also act as Lewis base sites, which can partly modulate the electronic properties, basicity and hydrophilicity of carbon black.[40,41] To the best of our knowledge, few works have been reported about the well-dispersed nitrogen-doped carbon black (NCB) supported bimetallic PdAu NPs in organic catalysis.

In this work, we report a facile, mild and surfactant-free process for the synthesis of a well-dispersed NCB supported bimetallic PdAu catalyst with an average particle size of 3.4 nm. The Pd/Au mole ratios can be easily tuned through controlling the amounts of the metal precursors. The PdAu/NCB catalyst with a Pd/Au ratio of 1/1 exhibits the most activity for both the Ullmann coupling reaction and the hydrogenation reaction of nitrophenols. Compared with the monometallic Pd/NCB or Au/NCB catalysts, the synergistic effect between two different metals and the combined effect between the nanoparticles and NCB lead to an enhanced catalytic performance, achieving a cost-effective Ullmann coupling reaction and nitrophenol hydrogenation reaction.

Experimental details

Materials

XC-72 carbon black (CB) was supplied by the Cabot Corporation. Bromobenzene (AR., 99%) and magnesium sulfate anhydrous ($MgSO_4$, AR.) were purchased from the Aladdin Industrial Cooperation. Ethylene glycol (EG, 99.0%), nitric acid (HNO_3, 65–68%), isopropanol (IPA) and potassium carbonate (K_2CO_3) were of analytical grade and purchased from Sinopharm Chemical Reagent Co., Ltd. L-Ascorbic acid (AR.) was purchased from Xilong Scientific Co., Ltd. Potassium tetrachloropalladate (K_2PdCl_4, 99.99%) and chloroauric acid ($HAuCl_4 \cdot 9H_2O$, 99.99%) were obtained from Alfa Aesar. All the chemicals in this work were used without further purification, and deionized water was used for the preparation of various solutions throughout the entire study.

Synthesis of PdAu/NCB

Nitrogen-doped carbon black (NCB) was first synthesized through a hydrothermal process according to our previous work.[42] Pd_xAu_y/NCB nanocatalysts with a metal loading of 10 wt% were fabricated through a co-reduction process in the liquid system, where x and y are the relative molar ratios of Pd and Au, respectively, and $x + y = 10$. Typically, 20 mg of NCB was dispersed in 20 mL of ethylene glycol (EG) with sonication for 10 min to obtain a uniform suspension. Then 5 mL of L-ascorbic acid (1.0 mg mL^{-1}) aqueous solution was dropped in with continuous stirring. After that, 5 mL of a fresh aqueous solution of metal precursors which contains the required amounts of K_2PdCl_4 and $HAuCl_4 \cdot 9H_2O$ was added into the above mixture with vigorous stirring at room temperature. After 2 h, the solid residue was filtered, washed with water and freeze-dried for further use, labelled as Pd_xAu_y/NCB. The schematic fabrication process is shown in Scheme 1.

According to the amounts of Pd and Au precursor in the solution, catalysts with different molar ratios of Pd : Au were obtained, and were set as 1 : 9, 3 : 7, 5 : 5, 7 : 3 and 9 : 1, respectively. Moreover, Pd/NCB and Au/NCB were also prepared in the same way but with only the Pd or Au precursor in the solution.

Characterization

The morphology and microstructure of the catalyst were characterized by transmission electron microscopy (TEM, JEOL JEM-2100). To further identify the state of Pd and Au in the nanohybrid, PdAu/NCB was observed by high-angle annular dark-field scanning TEM (HAADF-STEM) and energy dispersive X-ray spectroscopy (EDX) mapping analysis (Tecnai G2 F30 S-Twin TEM). The structure of the catalyst was characterized by X-ray diffraction (XRD, Bruker D8 Advance diffractometer) analysis using Cu Kα radiation ($\lambda = 0.15406$ nm). The chemical state of each element was obtained by X-ray photoelectron spectroscopy (XPS) spectra on a PHI-5000C ESCA system (Thermo ESCALAB 250) with an Al Kα X-ray ($E = 1486.6$ eV) as the excitation light source. The nitrogen adsorption–desorption isotherm and BJH pore size distribution were measured by using a TriStar II3020 automated gas adsorption analyzer at 77 K. Inductively Coupled Plasma Optical Emission Spectroscopy (ICP-OES) was performed on an ICP-OES analyzer (Agilent 730). The yield of biphenyl was measured by high-performance liquid chromatography (HPLC, Agilent 1260 Infinity, Eclipse XDB-C18 column) analysis according to an external standard method. The absorbance was measured by a UV-vis spectrophotometer (PERSEE TU-1900).

Ullmann coupling reaction

The Ullmann coupling reaction was carried out at 40 °C in air for 3 hours. Typically, 1.0 mmol of aryl halide (1 equiv.), 3.0 mmol of base (3 equiv.) and 4 mg of the as-obtained catalyst were added into a mixed solution of 4 mL of IPA and 4 mL of water. Parts of mixture were taken out every 30 minutes for determination with HPLC. For the optimization of the reaction

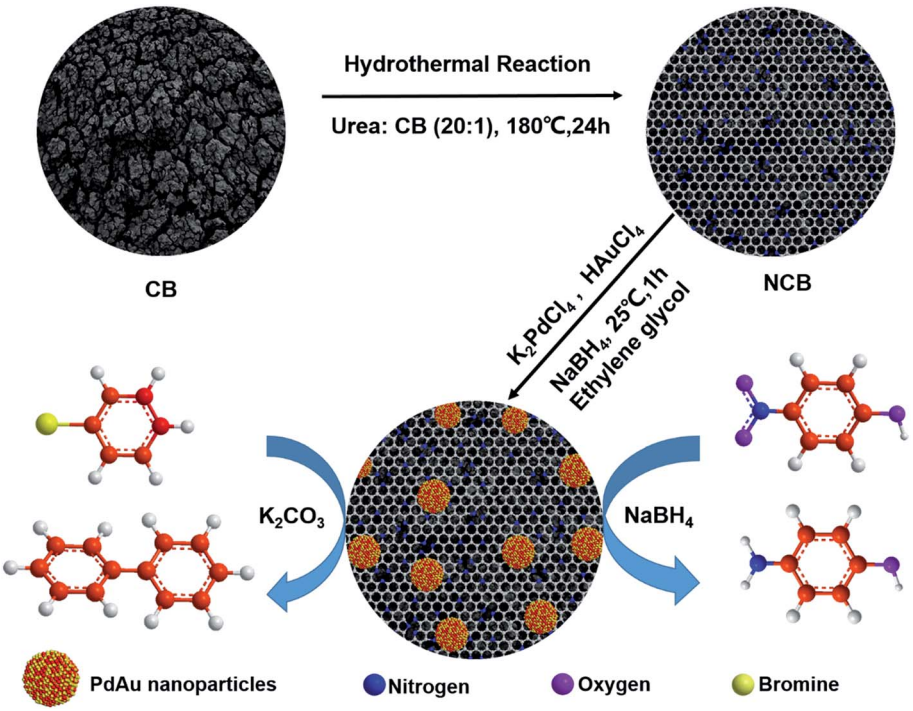

Scheme 1 Synthetic scheme of PdAu/NCB NPs for the Ullmann coupling of bromobenzene and reduction of 4-nitrophenol.

conditions, 200 μL of the above mixture was added into 4 mL of methanol followed by syringe filtration. The yield of biphenyl was measured by HPLC analysis according to an external standard method. While for the catalyst applicability study, the catalyst was removed by simple filtration, and then the remaining solution was extracted with ethyl acetate three times. The collected organic layers were combined, dehydrated with $MgSO_4$ and finally rotary evaporated. The resulting crude product was separated by column separation to give an isolated yield.

Nitrophenol hydrogenation reaction

Nitrophenol hydrogenation in the presence of an excess amount of $NaBH_4$ was carried out in an aqueous solution. Typically, 100 mg of $NaBH_4$ was mixed with the 20 mL of an aqueous solution of nitrophenol (100 mg L^{-1}), and then 85 μL of the catalyst suspension (1 mg catalyst/1 mL H_2O) was added to the above solution to start the reaction. In order to monitor the hydrogenation process, 3.0 mL of the solution was taken out of the reaction mixture at specific time intervals (2 minutes) followed by syringe filtration and finally measured by a UV-vis spectrophotometer to give time-dependent UV-vis spectra.

Results and discussion

Morphology and structure

As shown in Fig. 1A, the Pd_5Au_5 alloy nanoparticles are uniformly dispersed on the surface of the NCB, with an average particle size of 3.4 nm and a narrow size distribution ranging from 2 to 5 nm (Fig. 1B). The inset of 1A exhibits the high-resolution TEM image of the Pd_5Au_5/NCB catalyst. The lattice plane distance of the Pd_5Au_5 particle is estimated as 0.230 nm, which is between the lattice plane distance of Pd (111) and Au (111), 0.223 nm and 0.234 nm, respectively, indicating the formation of an alloy structure.[43,44] Furthermore, the elemental composition of the Pd_5Au_5/NCB was further investigated by the HAADF-STEM technique (Fig. 1C and D). The STEM-EDX mapping results confirm that C, N, O, Pd and Au elements are apparently observed in Pd_5Au_5/NCB. A homogeneous distribution of both Pd and Au is found (Fig. 1D), indicating the formation of a PdAu alloy on the surface of NCB.

XRD analysis was used to further study the structure of the catalysts. Fig. 2A shows the XRD patterns of NCB, Pd/NCB, Au/NCB and PdAu/NCB catalysts with different Pd–Au molar ratios. For all the PdAu/NCB catalysts with different Pd/Au molar ratios, a broad peak centered at $2\theta = 25°$ can be observed, which is ascribed to C (002) in the NCB material. As for Pd/NCB, the diffraction peaks centered at 2θ = 40.09°, 46.60°, 68.00° and 81.90° are assigned to the (111), (200), (220), and (311) lattice planes of face-centered cubic Pd, respectively. Similarly, for Au/NCB, the peaks located at 38.18°, 44.44°, 64.65°, 77.56° and 81.77 correspond to (111), (200), (220), (311) and (222). For the PdAu/NCB samples, an obvious shift (Fig. 2B) can be observed for the main peaks with an increase in the Pd content, suggesting the formation of a PdAu alloy rather than a core–shell structure.[45–47] Meanwhile, the decreased intensity of the peaks implies a lower crystallization degree.

The typical IUPAC type IV pattern with a hysteresis loop in Fig. 2C shows that the Pd_5Au_5/NCB has a Brunauer–Emmett–Teller (BET) surface area (S_{BET}) of 125.45 m^2 g^{-1} and a pore volume of 0.24 cm^3 g^{-1}. The corresponding pore size

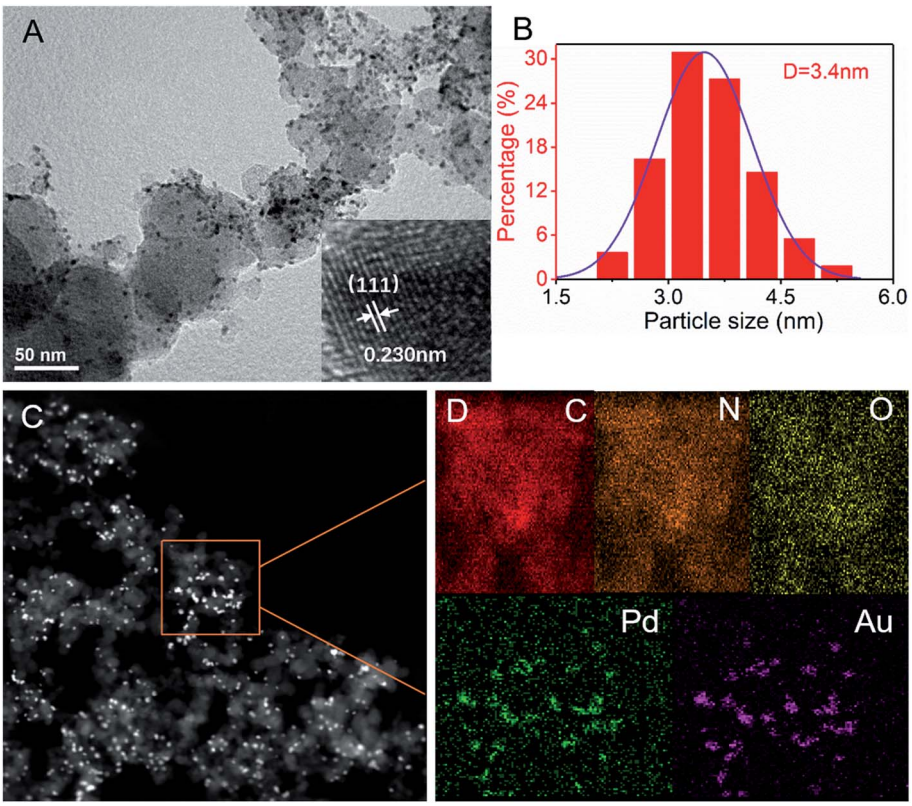

Fig. 1 (A) TEM image, the inset is a HRTEM image; (B) particle size distribution; (C) HAADF-STEM images of Pd_5Au_5/NCB; (D) EDS mapping of C, N, O, and Pd and Au element.

distribution (Fig. 2D) shows that the NCB material itself has a pore size of around 3.60 nm, while the mesopore with a size of 34.96 nm simply reflects the average size of the voids between the aggregated particles. According to these results, the large specific surface area and abundant pores are expected to enhance the catalytic performance.

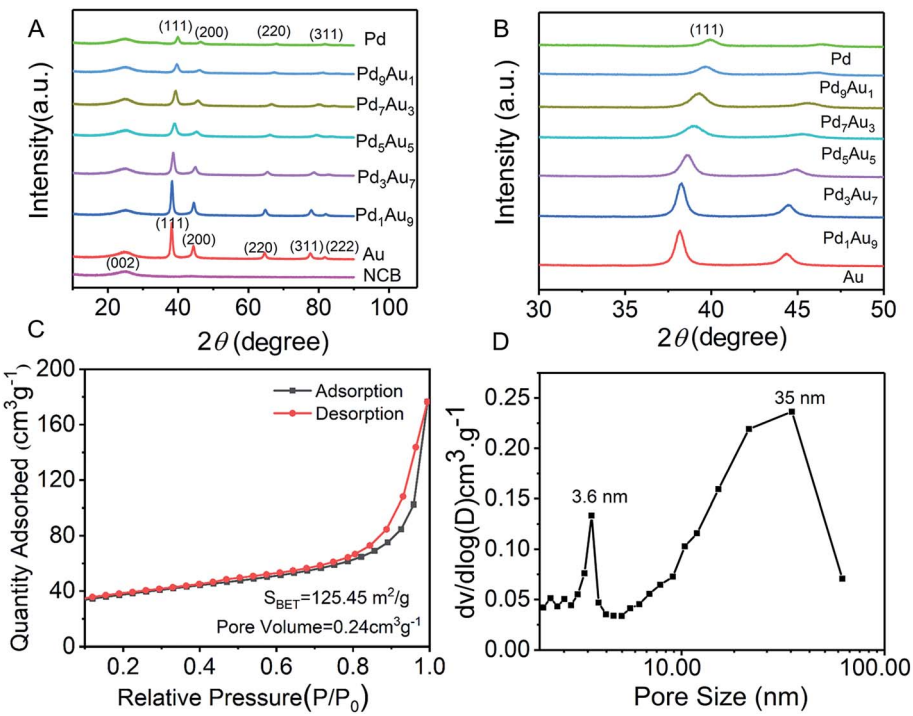

Fig. 2 (A) XRD patterns of NCB and PdAu/NCB with different Pd/Au molar ratios; (B) the enlarged XRD patterns between $2\theta = 30–50°$; (C) nitrogen adsorption–desorption isotherm; (D) BHJ pore size distribution of the Pd_5Au_5/NCB.

XPS characterization was employed to obtain the superficial element information of the as-prepared Pd_5Au_5/NCB catalyst. The XPS survey scans of Pd/NCB, Au/NCB and Pd_5Au_5/NCB are shown in Fig. 3A. The peaks of C, O, Pd and Au can be seen clearly on the Pd_5Au_5/NCB composite. Additionally, a weak peak of N 1s can also be observed, which indicates that nitrogen is successfully doped into carbon black *via* the facile hydrothermal treatment. The high-resolution XPS fitting spectrum of C 1s concludes that C exists in the form of a sp^2 C=C, a defect peak or sp^2 C=N, C–OH, C=O or C–N and O–C=O with the binding energy (BE) centered at 284.6, 285.2, 286.1, 287.1 and 289.1 eV, respectively (Fig. 3B).[48–50] The convoluted result of the N 1s spectra shows three types of N species, including pyridinic N (398.8 eV, 39.9%), pyrrolic nitrogen (399.8 eV, 48.7%) and amino functional groups (401.3 eV, 11.4%), respectively (Fig. 3C).[48,51] Also, the corresponding data of the atomic percentage of each nitrogen type indicated that the major nitrogen types in our support material are pyridinic N and pyrrolic N. As for the Au 4f spectrum of the Pd_5Au_5/NCB catalyst, it is well fitted with two pairs of peaks (Fig. 3D). One doublet located at 83.8 and 87.5 eV (ref. 52 and 53) is assigned to Au^0, while the other at BE = 84.9 and 88.6 eV corresponds to Au^+. Similarly, Pd^0 (BE = 340.3 and 335.1 eV), Pd^{2+} (BE = 336.5 and 341.7 eV) and Pd^{4+} (BE = 337.8 and 343.0 eV) are three typical Pd species that appear in the Pd_5Au_5/NCB composite[54,55] (Fig. 3E). It is worth noting that, compared with Au/NCB and Pd/NCB (Fig. 3D and E), both XPS spectra of Au 4f and Pd 3d in Pd_5Au_5/NCB have shifted to a lower binding energy, suggesting the electron transfer to Pd and Au metals. Due to the conductivity of NCB, we can deduce that these electrons came from NCB, confirming the interaction between PdAu NPs and NCB.[56] Compared with the PdAu/CB sample (Fig. S1†), the Pd and Au peak positions of PdAu/NCB shift to higher binding energies, which is attributed to the metal-support interaction (MSI)

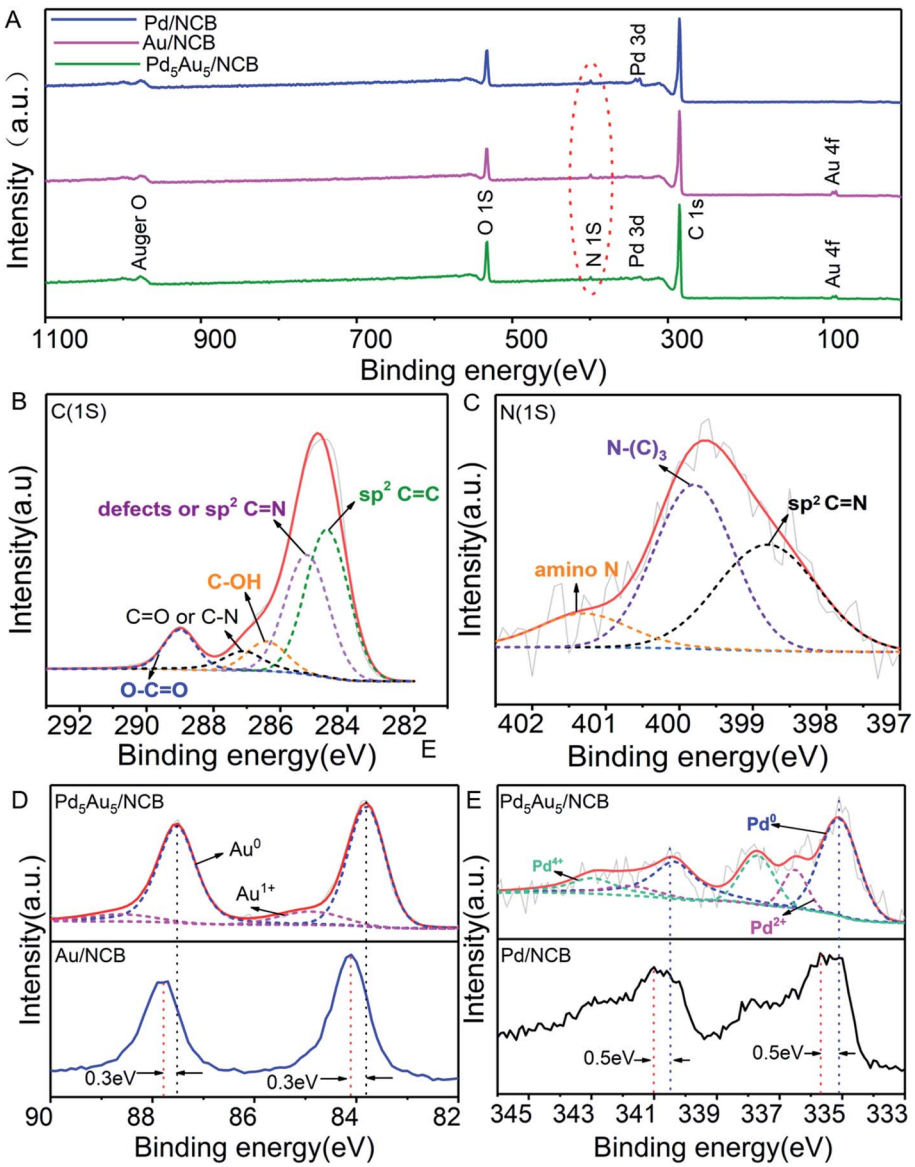

Fig. 3 (A) Global XPS spectrum of Pd_5Au_5/NCB; XPS spectra of C 1s (B), N 1s (C), Au 4f (D) and Pd 3d (E).

between PdAu nanoparticles and NCB,[57] suggesting an enhanced attraction force between the PdAu atoms and the NCB support.[48]

Ullmann coupling reaction

In our work, the Ullmann coupling of bromobenzene was employed as a model reaction to conduct the optimization of the reaction conditions with PdAu/CB and PdAu/NCB composites as the catalysts. The activities of PdAu/NCB with different Pd/Au molar ratios as well as their monometallic counterparts are summarized in Table 1. Monometallic Au/NCB was totally inactive for the Ullmann coupling of bromobenzene, and the monometallic Pd/NCB could only give a yield of 6%. Herein, it can be inferred that Pd is the only active site for the coupling reaction. By alloying Au with Pd, a great enhancement of the catalytic activity can be obtained. At an Au/Pd ratio of 5/5, the biphenyl yield reaches the highest value of 95% within 3 h. The yield of biphenyl over Pd_5Au_5/CB was only 16% under the same conditions. Hence, Pd_5Au_5/NCB was considered the best catalyst for further study.

As the bases and solvents play an important role in the Ullmann coupling reaction, a control variate method was employed to study the influence of each factor. As shown in Table 2, various bases, such as K_2CO_3, KOH, $NaHCO_3$, NH_4HCO_3, NaOH, C_5H_5N, HCOONa and Et_3N (entries 5–12), were employed in the Ullmann coupling reaction. Among these bases, K_2CO_3 was the most efficient for the Ullmann reaction in the IPA/H_2O system with a 94.6% yield of biphenyl (entry 12). So, we used K_2CO_3 as the base in the subsequent experiments because of its high efficiency and low cost. Organic solvents such as IPA, EtOH, C_4H_4O and H_2O gave moderate yields (entries 1–4). Interestingly, a mixed water-organic solvent can tremendously increase the yield of biphenyl (entries 12–14) in the presence of K_2CO_3 as a base, especially, the highest yield of 95% can be obtained by using the IPA/H_2O system (entry 12). Because the base and organic reactants are more easily dissolved in the mixed solutions, organopalladium intermediates are easily formed, thus facilitating the reaction. Additionally, the desired product of biphenyl will separate out because of its limited solubility in the IPA/H_2O medium, driving the reaction equilibrium in the forward direction. Hence, the IPA/H_2O system is considered to be the best solvent because it is safe, easily available and environmentally friendly. So, the optimized reaction conditions are as follows: bromobenzene (1 mmol), K_2CO_3 (3 mmol), Pd_5Au_5/NCB (4 mg), IPA (4 mL), and water (4 mL) at 40 °C for 3 h.

The generality of the catalyst for the Ullmann coupling reaction was examined by extending different bromobenzene derivatives containing electron-donating and electron-withdrawing functional groups under the optimized conditions. As shown in Table 3, the activity of 4-OCH_3-substituted aryl benzenes follows the sequence of I > Br > Cl because of the difference between the electronegativity of halogen atoms (Cl > Br > I), where higher electronegativity leads to a stronger carbon–halogen bond and thus a lower activity (entries 1–3).[58] This result is consistent with the work reported by Zhang *et al.*,[59] in which ion exchange resin supported Au alloyed with Pd single atoms was explored to serve as an effective and robust catalyst for the Ullmann reaction of aryl halides. For other OCH_3-substituted bromobenzenes (entries 4–5), the 2-OCH_3 substituted bromobenzene gives a lower yield of 85.1% due to steric hindrance.[60] Moreover, for *para*-position substituted aryl bromides with electron-donating (–OH and $–CH_3$) or electron-withdrawing (–CN, –CHO, $–NO_2$) functional groups, desirable yields can be obtained under required conditions (entries 6–10). In addition, 4-NO_2 iodobenzene can give the corresponding symmetrical products with a yield of 88.6% in 2 h (entry 11). However, Dhital *et al.*[24,61] reported that Au–Pd alloy nanoclusters stabilized by PVP could efficiently catalyze the Ullmann coupling of chloroarenes but not for bromoarenes and iodide arenes, and aryl iodide was a stronger inhibitor by forming a stable complex with a gold component. Obviously, the as-prepared PdAu/NCB catalysts are more stable and adaptable to different substrates.

A possible pathway for the Ullmann coupling of aryl halides catalyzed by the PdAu/NCB is proposed in Scheme 2. First, the aryl halides are adsorbed onto the surface of PdAu NPs followed by the activation (step A) and cleavage of the carbon–halogen (C–X) bond to generate metal-aryl and metal-halogen intermediates (step B). Later, a carbon–carbon bond is formed by

Table 1 Ullmann coupling of bromobenzene over PdAu/NCB catalysts with various Au/Pd ratios[a]

Catalyst	Au	Pd_1Au_9	Pd_3Au_7	Pd_5Au_5	Pd_7Au_3	Pd_9Au_1	Pd
Yield (%)	0	49	74	95	51	18	6

[a] Reaction conditions: bromobenzene (1 mmol), K_2CO_3 (3 mmol), IPA (4 mL), H_2O (4 mL), PdAu/NCB (4 mg, 10 wt% PdAu loading), 40 °C, 3 h.

Table 2 Optimization of the experimental conditions for the Ullmann coupling reaction of bromobenzene[a]

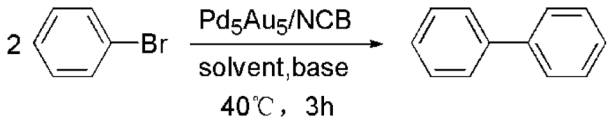

Entry	Base	Solvent (mL mL^{-1})	Yield (%)
1	K_2CO_3	IPA	52
2	K_2CO_3	EtOH	70
3	K_2CO_3	C_4H_4O	60
4	K_2CO_3	H_2O	52
5	KOH	IPA/H_2O = 4/4	55
6	$NaHCO_3$	IPA/H_2O = 4/4	30
7	NH_4HCO_3	IPA/H_2O = 4/4	10
8	Et_3N	IPA/H_2O = 4/4	8
9	NaOH	IPA/H_2O = 4/4	60
10	C_5H_5N	IPA/H_2O = 4/4	20
11	HCOONa	IPA/H_2O = 4/4	17
12	K_2CO_3	IPA/H_2O = 4/4	94
13	K_2CO_3	EtOH/H_2O = 4/4	82
14	K_2CO_3	C_4H_4O/H_2O = 4/4	75

[a] Reaction conditions: bromobenzene (1 mmol), base (3 mmol), solvent (8 mL), PdAu/NCB(4 mg, 10 wt% Pd_5Au_5 loading, the calculated moles of Pd_5Au_5 is 0.0013 mmol), 40 °C, 3 h. Yields were determined by HPLC according to the standard curve based on biphenyl.

Table 3 Generality of the Pd_5Au_5/NCB catalyst in the Ullmann coupling reaction involving different aryl halides[a]

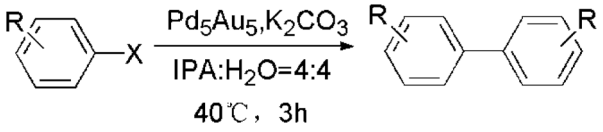

Entry	Aryl halide	Product	Time	Yield (%)
1	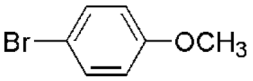	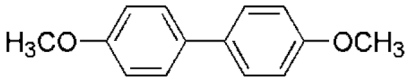	3 h	95
2	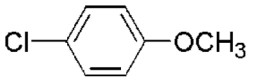	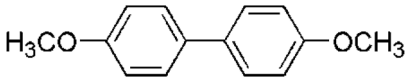	5 h	85
3	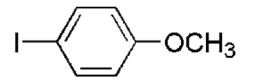	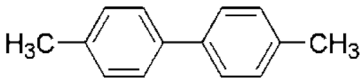	1 h	97
4	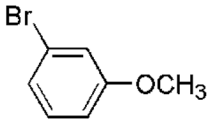	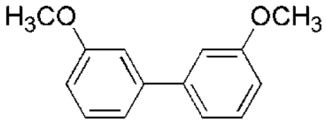	3 h	92
5	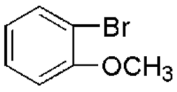	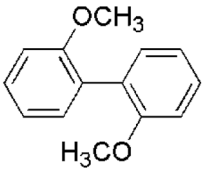	3 h	85
6	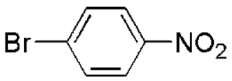	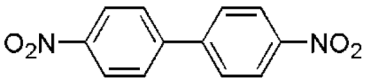	3 h	81
7	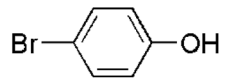	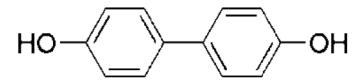	3 h	90
8	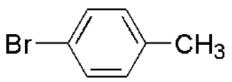	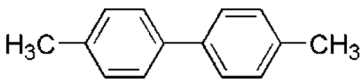	3 h	92
9	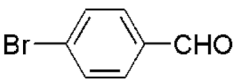	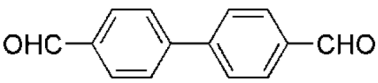	3 h	88
10	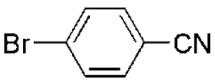	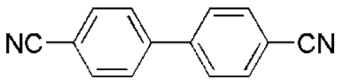	3 h	87
11	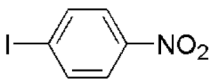	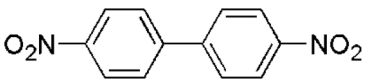	2 h	88

[a] Reaction conditions: aryl halide(1 mmol), K_2CO_3 (3 mmol), IPA (4 mL), H_2O (4 mL), Pd_5Au_5/NCB (4 mg, 10 wt% Pd_5Au_5 loading), 40 °C, 3 h, isolated yield.

reductive elimination (step C) and the bi-aryl product is desorbed from the active site and into the solution, accompanying the recovery of alloy nanoparticles by isopropanol (step D).[62–64] As demonstrated by many reports, alcohols (such as ethanol or isopropanol) can be used as reducing agents for Ullmann homocoupling.[65–67]

Based on the above investigation, the excellent activity of PdAu/NCB in Ullmann coupling can probably be attributed to the unique nanostructure of the catalyst and the synergistic effect between individual components: (1) the abundant oxygen containing functional groups and large surface area on of NCB could anchor the PdAu NPs, which is in favor of the dispersion and stability of the catalyst. Moreover, nitrogen-doping can increase the interaction between the PdAu and NCB, thus enhancing the catalytic durability.[68–70] (2) In the case of the Ullmann coupling reaction, Pd appears to be more catalytically active than Au. The synergistic effect creates highly active sites, which is beneficial to the oxidation addition of aryl halides.[52] (3)

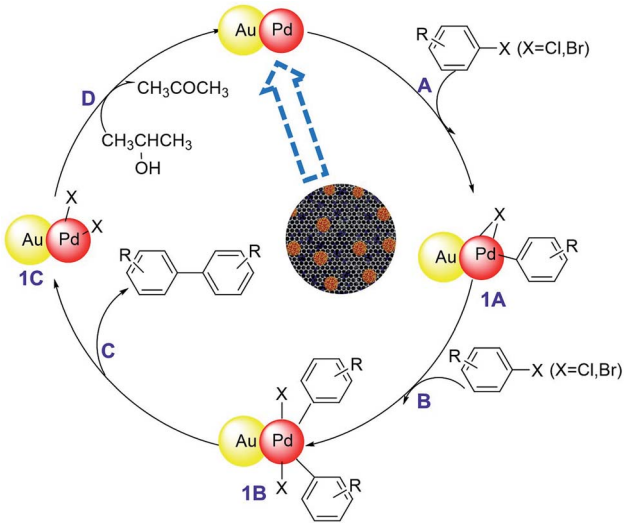

Scheme 2 Possible reaction pathway for the Ullmann coupling of aryl halides catalyzed by PdAu/NCB.

For the Ullmann coupling reaction itself, the almost biphenyl with a noncoplanar conjugated structure, poor polarity and limited solubility will quickly escape from the surface of the catalyst, driving the reaction in the forward direction.[71]

Hydrogenation of nitrophenols

The PdAu/NCB alloy catalyst is not only active for the Ullmann coupling reaction, but also behaves well in the hydrogenation reaction of nitro compounds. Here, the catalytic reduction of *p*-nitrophenol (4-NP) to *p*-aminophenol (4-AP) was set as a model reaction to estimate the activity of the catalysts. The reaction was carried out in an aqueous solution using an excess amount of $NaBH_4$ as the reductant. As shown in Fig. 4A, the maximum UV-vis adsorption wavelength of 4-NP is at 400 nm under alkaline conditions, while the peak maximum of 4-AP is around 303 nm.[53] In the presence of $NaBH_4$ and catalyst, the peak assigned to 4-NP decreases as the reaction proceeds, and meanwhile the peak of 4-AP increases concomitantly, which can be used to monitor the reaction process. Taking into account the excessive amount of $NaBH_4$, the pseudo-first-order kinetics related to 4-NP can be used to evaluate the kinetic rate constant, and the corresponding kinetic equation can be written as eqn (1):

$$\ln \frac{A}{A_0} = \ln \frac{c}{c_0} = -kt \quad (1)$$

where c is the concentration of 4-NP during the reaction, c_0 is the initial concentration of 4-NP, k is the rate constant and t is the reaction time.

Catalysts with different molar ratios of Pd and Au were synthesized in order to further investigate the catalytic activity for the hydrogenation of 4-NP to 4-AP. The $\ln c/c_0$ *vs.* reaction time over PdAu/NCB with various Pd/Au molar ratios is shown in Fig. 4B. Combining the results of Fig. 4B with Table 4, we can clearly conclude that all of the PdAu catalysts showed a higher catalytic activity compared with the corresponding Pd/NCB and Au/NCB, indicating the synergistic effect between Pd and Au nanoparticles in the PdAu alloy. Notably, the Pd_5Au_5/NCB catalyst exhibited the highest catalytic activity within 12 min to finish the reaction. However, only a 20% conversion of 4-NP could be obtained over Pd_5Au_5/CB within 12 min [Fig. S2†]. Obviously, N-doping can improve the catalytic performance due to an enhanced attraction force between PdAu atoms and the NCB support.[48,57]

We also investigate the effect of temperature on the hydrogenation reaction. Four different temperatures ranging from 20 to 35 °C were chosen for the reduction of 2-NP, 3-NP and 4-NP. The activation energy (E_a) can be calculated according to the Arrhenius equation (eqn (2)):

$$\ln k = \frac{-E_a}{RT} + \ln A \quad (2)$$

where k is the rate constant, E_a is the activation energy, R is the ideal gas constant (8.314 J mol^{-1} K^{-1}), T is the temperature, and A is the Arrhenius factor. As shown in Fig. 5 and Table 4, a larger k was achieved at a higher temperature. The k values of the 2-NP, 3-NP and 4-NP reduction were calculated as 0.2071, 0.1971 and 0.2114 min^{-1}, respectively, at 298.15 K. The activation energies (E_a) of the catalytic reduction for 2-NP, 3-NP and 4-NP over Pd_5Au_5 are calculated to be 55.12, 65.13 and 20.88 kJ mol^{-1},

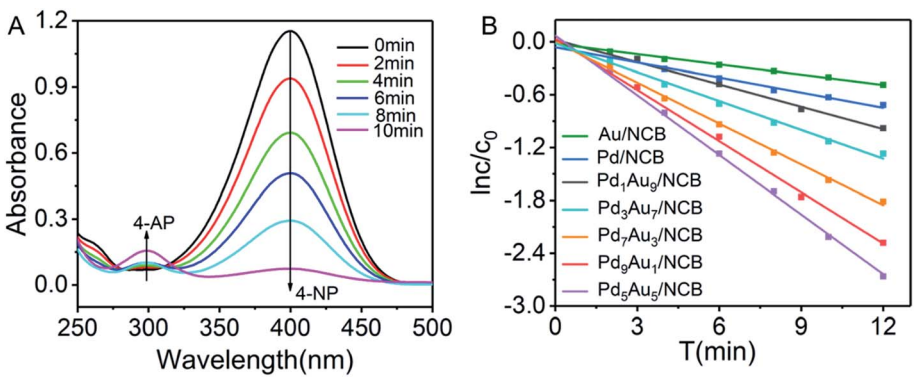

Fig. 4 (A) UV-vis adsorption spectra of 4-NP catalyzed by Pd_5Au_5/NCB at certain time intervals; (B) pseudo-first-order plot of $\ln(c/c_0)$ against reaction time for the hydrogenation of 4-NP over different catalysts.

Table 4 Pseudo-first-order kinetics constants for the 4-NP reduction of different catalysts[a]

Entry	Catalyst	k (min^{-1})	R^2
1	Pd_5Au_5/NCB	0.2895	0.9961
2	Pd_9Au_1/NCB	0.1930	0.9724
3	Pd_7Au_3/NCB	0.1543	0.9813
4	Pd_3Au_7/NCB	0.1137	0.9902
5	Pd_1Au_9/NCB	0.0872	0.9893
6	Pd/NCB	0.0575	0.9785
7	Au/NCB	0.0372	0.9812

[a] Reaction conditions: 4-NP (20 mL, 100 mg L^{-1}), catalyst suspension (85 μL, 1 mg mL^{-1}), $NaBH_4$ (50 mg), 25 °C.

respectively. Obviously, 4-NP exhibits the lowest activation energy and the highest rate constant k.

Thermodynamic parameters, including the activation of entropy ($\Delta S^{\#}$), enthalpy ($\Delta H^{\#}$) and Gibbs energy change ($\Delta G^{\#}$), are calculated following eqn (3) and (4), where k_B is the Boltzmann constant (1.38×10^{-23} J K^{-1}) and h is the Planck constant (6.63×10^{-34} J).[72] For Pd_5Au_5/NCB, the values of $\Delta S^{\#}$, $\Delta H^{\#}$ and $\Delta G^{\#}$ are listed in Table 5. The positive values of activation of enthalpy show that the reduction of 2-NP, 3-NP and 4-NP is an endothermic reaction and the positive $\Delta G^{\#}$ values indicate that the hydrogenation needs the catalyst.[73] The negative entropy ($\Delta S^{\#}$) values indicate that randomness on the catalyst-solution interface decreased during the catalytic reduction process.[74] In addition, the $\Delta G^{\#}$ values increase as the temperature rises, which indicates that the reduction process of 2-NP, 3-NP and 4-NP needs energy.[75–77]

$$\ln\left(\frac{k}{T}\right) = \ln\left(\frac{k_B}{h}\right) + \frac{\Delta S^{\#}}{R} - \frac{\Delta H^{\#}}{R}\left(\frac{1}{T}\right) \quad (3)$$

$$\Delta G^{\#} = \Delta H^{\#} - T\Delta S^{\#} \quad (4)$$

Based on the experimental results and the literature,[78,79] the high activity of Pd_5Au_5/NCB can be attributed to a synergistic effect and the unique nanostructure. The nitro group as an electron-withdrawing group enhances the π–π stacking interactions by reducing the electron density of π electrons, diminishing the repulsive electrostatic interactions between the aromatic rings.[80] It provides a higher concentration of nitrophenol molecules near to the PdAu NPs on N-doping carbon black, leading to a highly efficient contact between the reactant molecules and the active sites, thus enhancing activity.[81]

Cycling performance

The recoverability and reusability of the catalyst are of great importance. The Pd_5Au_5/NCB was used in the Ullmann coupling of bromobenzene at 40 °C and the reduction of 4-NP at 25 °C over 10 cycles. As shown in Fig. 6, both the conversion efficiency of 4-NP and yield of the Ullmann coupling over Pd_5Au_5/NCB maintained at over 80%, suggesting a good reusability of Pd_5Au_5/NCB in the reaction.

The recovered catalyst was re-characterized using XPS, TEM HAADF and ICP. XPS analysis (Fig. S3†) reveals that PdAu nanoparticles maintain their state after the tenth use. TEM HAADF images of the tenth cycle of catalysis (Fig. S4†) show the

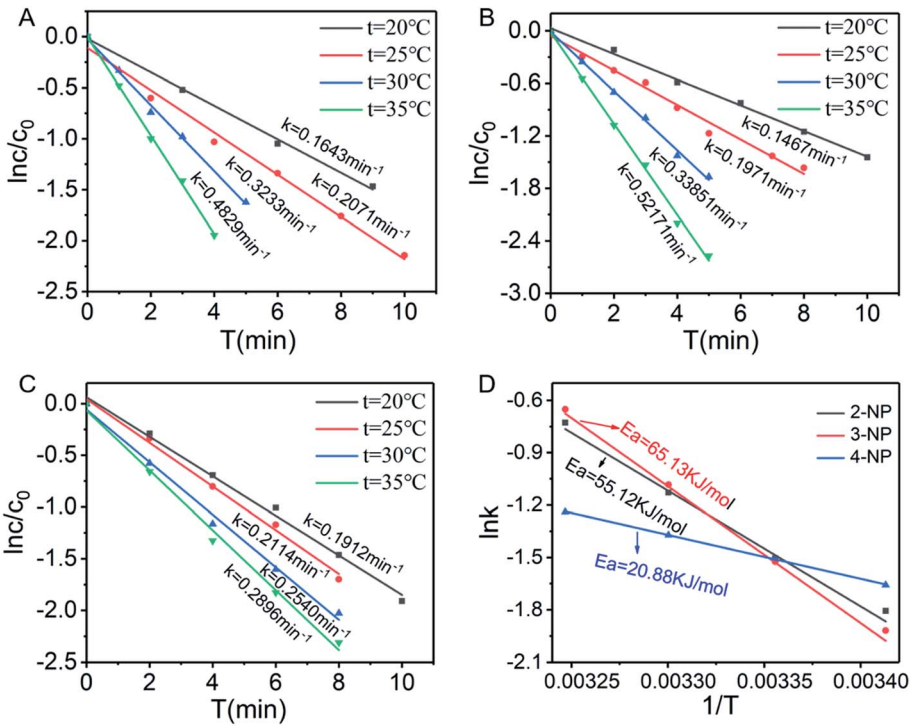

Fig. 5 Pseudo-first-order plot of ln c/c_0 against reaction time for the reduction of 2-NP (A), 3-NP (B) and 4-NP (C) catalyzed by Pd_5Au_5; plot of ln k against $1/T$ for the reduction of 2-NP, 3-NP and 4-NP (D).

Table 5 Kinetic and thermodynamics parameters of catalytic reaction for 2-NP, 3-NP and 4-NP over Pd_5Au_5/NCB

Substrate	T (K)	K (min^{-1})	E_a (kJ mol^{-1})	ΔH (kJ mol^{-1})	ΔS (J mol^{-1} K^{-1})	ΔG (kJ mol^{-1})
2-NP	293	0.1643	55.12	44.8	−122.34	80.64
	298	0.2071				81.25
	303	0.3233				81.86
	308	0.4829				82.48
3-NP	293	0.1467	65.13	57.1	−80.6	80.31
	298	0.1971				80.71
	303	0.3385				81.11
	308	0.5217				81.52
4-NP	293	0.1912	20.88	19.13	−212.9	82.58
	298	0.2114				84.70
	303	0.2540				86.83
	308	0.2896				88.96

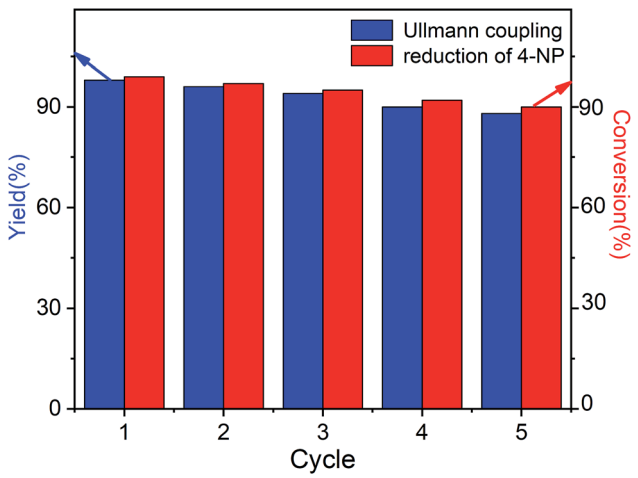

Fig. 6 Cycling performance of Pd_5Au_5/NCB for the reduction of 4-NP and the Ullmann coupling of bromobenzene.

PdAu particles had slightly grown to 4–6 nm, indicating the mild agglomeration of the particles, which may have caused the reduction in the catalytic activity after the tenth use. Metal leaching of the catalyst before and after the reaction was studied using ICP. The Au and Pd contents of the Pd_5Au_5/NCB are shown in Table S1† before reaction and after ten reaction cycles. These results demonstrate that the amount of metal loss can be 5%, which may be cause the decrease of the activity of Pd_5Au_5/NCB NPs.[82]

Furthermore, we performed a filtration test in the Ullmann coupling of PhBr at 40 °C. The Pd_5Au_5/NCB was filtrated out using a syringe filter after 1 h. As indicated in Fig. S5,† the catalytic reaction did not occur after the catalyst was filtered, which confirmed the heterogeneous nature of the catalysis.

Conclusion

In summary, a series of PdAu alloy catalysts was prepared with N-doped carbon black as the support *via* a co-reduction method. Due to the surfactant-free formation process, the PdAu/NCB catalysts are clean, and effective for the Ullmann coupling of aryl halides and for nitrophenol hydrogenation. According to the results, the PdAu/NCB nanoparticles are more active compared to the corresponding monometallic counterparts; moreover, Pd_5Au_5/NCB exhibits the highest activity. The price of the catalyst is low due to the low price of NCB. The enhanced catalytic performance can be ascribed to the unique nanostructure of the catalyst including the large BET surface, small size of PdAu NPs, excellent PdAu dispersion, strong adsorption of organic molecules on the surface of NCB, and the synergistic effect between two different metals and the combined effect between the nanoparticles and NCB.

Conflicts of interest

There are no conflicts to declare.

Acknowledgements

This work was supported by the Fundamental Research Funds for the Central Universities (No. 30916014103), NSF of China (No. 51572125), the Natural Science Foundation of Jiangsu Province (No. BK20171423) and PAPD of Jiangsu.

References

1 J. Hassan, M. Sévignon, C. Gozzi, E. Schulz and M. Lemaire, *Chem. Rev.*, 2002, **102**, 1359–1470.
2 R. Martin and S. L. Buchwald, *Acc. Chem. Res.*, 2008, **41**, 1461–1473.
3 F. Yang, Y. Li, T. Liu, K. Xu, L. Zhang, C. Xu and J. Gao, *Chem. Eng. J.*, 2013, **226**, 52–58.
4 N. Miyaura and A. Suzuki, *Chem. Rev.*, 1995, **95**, 2457–2483.
5 Y. Yin and J. Liebscher, *Chem. Rev.*, 2007, **107**, 133–173.
6 S. Y. Xu, Y. B. Ruan, X. X. Luo, Y. F. Gao, J. S. Zhao, J. S. Shen and Y. B. Jiang, *Chem. Commun.*, 2010, **46**, 5864–5866.
7 M. Opanasenko, P. Stepnicka and J. Cejka, *RSC Adv.*, 2014, **4**, 65137–65162.
8 G. Cravotto, M. Beggiato, A. Penoni, G. Palmisano, S. Tollari, J. M. Lévêque and W. Bonrath, *Tetrahedron Lett.*, 2005, **46**, 2267–2271.

9 L. Shao, Y. Du, M. Zeng, X. Li, W. Shen, S. Zuo, Y. Lu, X. M. Zhang and C. Qi, *Appl. Organomet. Chem.*, 2010, **24**, 421–425.
10 Z. Zhou and W. Xue, *J. Organomet. Chem.*, 2009, **694**, 599–603.
11 A. P. I. BhatI, F. Inam and B. R. Bhat, *RSC Adv.*, 2013, **3**, 22191–22198.
12 J. Long, Y. Zhou and Y. Li, *Chem. Commun.*, 2015, **51**, 2331–2334.
13 W. Zhao, L. Dong, C. Huang, Z. M. Win and N. Lin, *Chem. Commun.*, 2016, **52**, 13225–13228.
14 F. Gao and D. W. Goodman, *Chem. Soc. Rev.*, 2012, **4**, 8009–8020.
15 X. W. Teng, Q. Wang, P. Liu, W. Q. Han, A. I. Frenkel, W. Wen, N. Marinkovic, J. C. Hanson and J. A. Rodriguez, *J. Am. Chem. Soc.*, 2008, **130**, 1093–1101.
16 Y. Sohn, D. Pradhan and K. T. Leung, *ACS Nano*, 2010, **4**, 5111–5120.
17 S. Zhang, Y. Y. Shao, H. G. Liao, J. Liu, I. A. Aksay, G. P. Yin and Y. H. Lin, *Chem. Mater.*, 2011, **23**, 1079–1081.
18 M. Sankar, N. Dimitratos, P. J. Miedziak, P. P. Wells, C. J. Kielye and G. J. Hutchings, *Chem. Soc. Rev.*, 2012, **41**, 8099–8139.
19 S. Sarina, S. Bai, Y. Huang, C. Chen, J. Jia, E. Jaatinen, G. A. Ayoko, Z. Bao and H. Zhu, *Green Chem.*, 2014, **16**, 331–341.
20 N. Agarwal, S. J. Freakley, R. U. McVicker, S. M. Althahban, N. Dimitratos, Q. He, D. J. Morgan, R. L. Jenkins, D. J. Willock, S. H. Taylor, C. J. Kiely and G. J. Hutchings, *Science*, 2017, **358**, 223–227.
21 J. W. Xia, Y. S. Fu, G. Y. He, X. Q. Sun and X. Wang, *Appl. Catal., B*, 2017, **200**, 39–46.
22 H. Jing and H. Wang, *Chem. Mater.*, 2015, **27**, 2172–2180.
23 J. J. Lv, Z. J. Wang, J. J. Feng, R. Qiu, A. J. Wang and X. Xu, *Appl. Catal., A*, 2016, **522**, 188–193.
24 R. N. Dhital, C. Kamonsatikul, E. Somsook, K. Bobuatong, M. Ehara, S. Karanjit and H. Sakurai, *J. Am. Chem. Soc.*, 2012, **134**, 20250–20253.
25 Z. J. Wang, X. Wang, J. J. Lv, J. J. Feng, X. H. Xu, A. J. Wang and Z. W. Liang, *New J. Chem.*, 2017, **41**, 3894–3901.
26 J. Wang, A. J. Xu, M. L. Jia, S. Bai, X. D. Cheng and B. Zhao, *New J. Chem.*, 2017, **41**, 1905–1909.
27 W. Fang, Y. C. Deng, L. Tang, G. M. Zeng, Y. Y. Zhou, X. Xie, J. J. Wang and Y. Wang, *J. Colloid Interface Sci.*, 2017, **490**, 834–843.
28 H. L. Jiang, T. Akita, T. Ishida, M. Haruta and Q. Xu, *J. Am. Chem. Soc.*, 2011, **133**, 1304–1306.
29 X. M. Chen, Z. X. Cai, X. Chen and M. Oyama, *J. Mater. Chem. A*, 2014, **2**, 5668–5674.
30 R. Bajpai, S. Roy S, P. Kumar, P. Bajpai, N. Kulshrestha, J. Rafiee, N. Koratkar and D. S. Misra, *ACS Appl. Mater. Interfaces*, 2011, **3**, 3884–3889.
31 L. Perini, C. Durante, M. Favaro, V. Perazzolo, S. Agnoli, O. Schneider, G. Granozzi and A. Gennaro, *ACS Appl. Mater. Interfaces*, 2015, **7**, 1170–1179.
32 D. T. Liu, W. James and A. M. Rami, *Nat. Geosci.*, 2017, **10**, 184–188.
33 J. Yan, T. Wei and B. Shao, *Carbon*, 2010, **48**, 1731–1737.
34 P. J. Li, J. H. Wu and J. M. Lin, *Sol. Energy*, 2009, **83**, 845–849.
35 J. Liu, P. Song and W. Xu, *Carbon*, 2017, **115**, 763–772.
36 V. Z. Radkevich, T. L. Senko, K. Wilson, L. M. Grishenko, A. N. Zaderko and V. Y. Diyuk, *Appl. Catal., A*, 2008, **335**, 241–251.
37 M. Zhu and G. Diao, *Nanoscale*, 2011, **3**, 2748–2767.
38 Z. Li, J. Liu, Z. Huang, Y. Yang, C. Zia and F. Li, *ACS Catal.*, 2013, **3**, 839–845.
39 A. A. Deshmukh, R. U. Islam, M. J. Witcomb, W. A. Otterlo and N. J. Coville, *ChemCatChem*, 2010, **2**, 51–54.
40 N. Sun, M. L. Wang and J. F. Chang, *Front. Energy*, 2017, **11**, 310–317.
41 Y. Z. Dong and J. H. Li, *Chem. Commun.*, 2015, **51**, 572–575.
42 J. W. Xia, Y. S. Fu, G. Y. He, X. Q. Sun and X. Wang, *Mater. Chem. Phys.*, 2018, **209**, 86–94.
43 S. H. Wang, Z. L. Xin, X. H. Huang, W. Z. Yu and S. N. Niu, *Phys. Chem. Chem. Phys.*, 2017, **19**, 6164–6168.
44 W. Hong, J. Wang and E. Wang, *ACS Appl. Mater. Interfaces*, 2014, **6**, 9481–9487.
45 X. Y. Liu, A. Q. Wang, X. Q. Mou and T. Zhang, *Chem. Commun.*, 2008, **44**, 3187–3189.
46 W. J. Li, A. Q. Wang, X. Y. Liu and T. Zhang, *Appl. Catal., A*, 2012, **433**, 146–151.
47 L. L. Zhang, A. Q. Wang, J. T. Miller, X. Y. Liu, X. F. Yang, W. T. Wang, L. L. Li, Y. Q. Huang, C. Y. Mou and T. Zhang, *ACS Catal.*, 2014, **4**, 1546–1553.
48 H. Y. Qian, H. J. Huang and X. Wang, *J. Power Sources*, 2015, **275**, 734–741.
49 Y. Wang, Y. Y. Shao, D. W. Matson, J. H. Li and Y. H. Lin, *ACS Nano*, 2010, **4**, 1790–1798.
50 G. Z. Hu, F. Nitze, T. Sharifi, H. R. Barzegara and T. Wågberg, *J. Mater. Chem.*, 2012, **22**, 8541–8548.
51 J. W. Xia, L. L. Zhang, Y. S. Fu, G. Y. He, X. Q. Sun and X. Wang, *J. Mater. Sci.*, 2018, **53**, 4467–4481.
52 C. H. Liu, R. H. Liu, Q. J. Sun, J. B. Chang, X. Gao, Y. Liu, S. T. Lee, Z. H. Kang and S. D. Wang, *Nanoscale*, 2015, **7**, 6356–6362.
53 A. Villa, N. Dimitratos, C. E. Chan-Thaw, C. Hammond, G. M. Veith, D. Wang, M. Manzoli, L. Prati and G. J. Hutchings, *Chem. Soc. Rev.*, 2016, **45**, 4953–4994.
54 L. S. Kibis, A. I. Stadnichenko, S. V. Koscheev, V. I. Zaikovskii and A. I. Boronin, *J. Phys. Chem. C*, 2012, **116**, 19342–19348.
55 X. N. Guo, P. Brault, G. J. Zhi, A. Caillard, G. Q. Jin, C. Coutanceau, S. Baranton and X. Y. Guo, *J. Phys. Chem. C*, 2011, **115**, 11240–11246.
56 X. M. Chen, Z. X. Cai, X. Chen and M. Oyama, *J. Mater. Chem. A*, 2014, **2**, 5668–5675.
57 Z. Y. He, B. Q. Dong, W. Wang, G. X. Yang, Y. H. Cao, H. J. Wang, Y. H. Yang, Q. Wang, F. Peng and H. Yu, *ACS Catal.*, 2019, **9**, 2893–2901.
58 L. Zhang, C. Feng, S. Gao, Z. Wang and C. Wang, *Catal. Commun.*, 2015, **61**, 21–25.
59 L. L. Zhang, A. Q. Wang, J. Miller, X. F. Yang, W. T. Wang, L. Li, Y. Q. Huang, C. Y. Mou and T. Zhang, *ACS Catal.*, 2014, **4**, 1546–1553.

60 H. Song, Q. Zhu, X. Zheng and X. Chen, *J. Mater. Chem. A*, 2015, **3**, 10368–10377.
61 R. N. Dhital, C. Kamonsatikul, E. Somsook, Y. Satod and H. Sakurai, *Chem. Commun.*, 2013, **49**, 2542–2544.
62 C. Kamonsatikul, T. Khamnaen and P. Phiriyawirut, *Catal. Commun.*, 2012, **26**, 1–5.
63 J. Wang, A. X. Xu, M. L. Jia, S. Bai, X. D. Cheng and G. T. Zhao, *New J. Chem.*, 2017, **41**, 1905–1910.
64 M. F. Zeng, Y. J. Du, L. J. Shao, C. Z. Qi and X. M. Zhang, *J. Org. Chem.*, 2010, **75**, 2556–2563.
65 J. Hassan, V. Penalva, L. Lavenot, C. Gozzi and M. Lemaire, *Tetrahedron*, 1998, **54**, 13793–13804.
66 L. Shao, Y. Du, M. Zeng, X. Li, W. Shen, S. Zuo, Y. Lu, X. Zhang and C. Qi, *Appl. Organomet. Chem.*, 2010, **24**, 421–425.
67 B. Z. Yuan, Y. W. Li, B. L. Yin and H. F. Jiang, *Angew. Chem., Int. Ed.*, 2010, **49**, 4054–4058.
68 Y. K. Zhou, K. Neyerlin, T. S. Olson, S. Pylypenko, J. Bult, H. N. Dinh, T. Gennett, Z. P. Shao and R. O'Hayre, *Energy Environ. Sci.*, 2010, **3**, 1437–1446.
69 K. Kakaei and K. Marzang, *J. Colloid Interface Sci.*, 2016, **462**, 148–153.
70 N. Liu, L. Z. Ding, M. J. Jia, W. X. Zhang, N. H. An and X. L. Yuan, *J. Colloid Interface Sci.*, 2017, **490**, 677–684.
71 S. I. Yamamoto, H. Kinoshita, H. Hashimoto and Y. Nishina, *Nanoscale*, 2014, **6**, 6501–6505.
72 V. K. Gupta, N. Atar, M. Yola, Z. Üstündag and L. Uzun, *Water Res.*, 2014, **48**, 210–217.
73 P. C. Guo, L. Tang, J. Tang, G. M. Zeng, B. B. Huang, H. R. Dong, Y. Zhang, Y. Y. Zhou, Y. C. Deng, L. L. Ma and S. R. Tan, *J. Colloid Interface Sci.*, 2016, **469**, 78–85.
74 V. K. Gupta, N. Atar, M. L. Yola, Z. Üstündağ and L. Uzun, *Water Res.*, 2014, **48**, 210–217.
75 M. Kohantorabi and M. R. Gholami, *Ind. Eng. Chem. Res.*, 2017, **56**, 1159–1167.
76 T. Zhou, T. T. Liu, Z. Q. Zhang, G. D. Zhang, F. W. Wang, X. F. Wang, S. Z. Liu, H. Z. Zhang, S. S. Wang and J. Ma, *J. Solid State Chem.*, 2018, **263**, 11–17.
77 M. Kohantorabi and M. R. Gholami, *Appl. Phys. A*, 2018, **124**, 441–445.
78 C. Wen, A. Yin and W. Dai, *Appl. Catal., B*, 2014, **160**, 730–741.
79 X. Li, K. Wu, Y. Ye and X. Wei, *Nanoscale*, 2013, **5**, 3648–3653.
80 Q. S. Liu, T. Zheng, P. Wang, J. P. Jiang and N. Li, *Chem. Eng. J.*, 2010, **157**, 348–356.
81 J. W. Xia, G. Y. He, L. L. Zhang, X. Q. Sun and X. Wang, *Appl. Catal., B*, 2016, **180**, 408–415.
82 H. Park, D. A. Reddy, Y. Kim, S. Lee, R. Ma, M. Lim and T. K. Kim, *Appl. Surf. Sci.*, 2017, **401**, 314–322.